Synthesis of a post-modified covalent organic framework as "turn-on" fluorescent chemosensor for highly selective and sensitive quantitative detection of common trivalent metal ions

Zeeshan Ali[a,b§], Xilan Li[a§], Uzma Sattar[b], Guang Wang[a,b*]

[a]School of Life Sciences, Zhuhai College of Science and Technology, Zhuhai, 519080, P.R. China

[b]Faculty of Chemistry, Northeast Normal University, Changchun 130024, PR China

§ These authors have contributed equally to this work.

Corresponding author: Guang Wang

Tel: 86+431+85099371;

Fax: 86+431+85098768.

E-mail：wangg923@nenu.edu.cn (G. Wang)

Table of Contents

Experimental Detail

Chemicals and instrumentation

Unless otherwise specified, all the reagents and chemicals acquired from commercial suppliers and utilized without further purification. All the measurements were taken at room temperature. The characterization of Py-Np COF and Ac-Py-Np COF had been performed in detail. Ultrapure water from Milli-Q water purification system was utilized in all the experiments. A Nicolet IS50 Fourier transform infrared spectrometer was used to record the Fourier transform infrared (FT-IR) spectra. The X-ray photoelectron spectroscopy (XPS) analysis was carried out using a VG Multilab 2000 system equipped with Al Ka radiation. Bruker AVANCE III 400 WB spectrometer was used for ^{13}C CP/MAS NMR in solid state using a magnetic field of 9.39 T with a 4 mm standard bore CPM AS probe head at 297K. A Rigaku Dmax 2200 PC diffractometer was utilized to perform PXRD measurements. The morphology of Py-Np COF and Ac-Py-Np COF was observed utilizing field emission scanning electron microscopy (SEM, Philips XL30). Transmission electron microscopy (TEM) images were acquired using a Tecnai G2 F20 S-TWIN electron microscope (USA). The N_2 adsorption and desorption isotherms and pore size distribution were obtained at 77 K with an Autosorb iQ2 adsorptometer. The METTLER-TOLEDO TG/DTA analyzer was utilized for thermogravimetric analysis (TGA). UV-vis absorption spectra data was taken from a Varian Cary 500 Spectrophotometer. Fluorescence spectra was measured on an F-4600 spectrometer (Hitachi, Japan). The fluorescence lifetime analysis was performed on Edinburgh Fluorescence Spectrometer (FLS920P). The simulated structure of Py-Np COF and Ac-Py-Np COF was obtained using Material Studio. DFT calculations were performed on Dmole[3] on Material Studio software.

Synthesis of Py-Np COF

The previously reported Py-Np COF was synthesized via solvothermal method under mild conditions. To reticulate Py-Np COF, the Pyrex tube was charged with (Py) 4,4',4",4'"-(pyrene-1,3,6,8-tetrayl)tetraaniline (22.67 mg, 0.04 mmol) and (Np) naphthalene-2,6-dicarbaldehyde (14.74 mg, 0.08 mmol) and added n-butanol (1.2 mL), 1,2-dichlorobenzene (1.2 mL) and aqueous acetic acid (6M, 240 µL). Then, the tube was sonicated for 30 minutes and degassed in the nitrogen atmosphere for consecutive three nitrogen thaw cycles. Afterwards, the Pyrex tube was sealed and heated at 120 ℃ for 72 hours in the simple oven. Next, the precipitates were collected by breaking

the tube at the neck, soaking for 20 minutes in the tetrahydrofuran (THF), followed by washing with THF and acetone three times. At last, yellow precipitates were obtained and dried at 60 ℃ in high-vacuum oven for 12 hours with the yield 89 %.

Synthesis of L-ascorbic acid modified COF

Ac-Py-Np COF was synthesized by immersing the Py-Np COF (30 mg) in 0.1 M aqueous L-ascorbic acid (5 mL) followed by vigorous shaking. The grafting of L-ascorbic acid can be visualized by instant color changing from yellow to blackish brown as shown in video.

Stock solutions preparation

10.0 mg of Ac-Py-Np COF was dispersed in different solvents (200 mL) and sonicated for 30 minutes. Aqueous solution of different metal ions Al^{3+}, Fe^{3+}, Cr^{3+}, Ag^{+}, Cu^{2+}, Hg^{2+}, Ga^{3+}, Fe^{2+}, $Sr^{2+,}$ Sn^{2+}, In^{3+}, $Li^{,}$ Na^{+}, Pb^{2+}, Zn^{2+}, Ba^{2+}, Mn^{2+}, $K^{+,}$ Co^{2+}, Mg^{2+}, Ca^{2+}, Ni^{2+}, Cd^{2+} were prepared utilizing their corresponding salts.

Preparation of chicken, mutton and kale samples

Fresh chicken and mutton (muscle tissue), and kale leaves were purchased from the super market. During sample preparation, 5.0 g of chicken, mutton and kale were separately measured with precision and 100 mL of distilled water was poured in each sample. Next, these samples were mixed in a homogenizer and boiled. 10 mL of 50 % nitric acid was added in each sample to dissolve them, and the mixtures were swirl continuously for 20 min. After that, these samples were left at room temperature for 30 min following by centrifugation at 8000 rpm for 5 min. The supernatants of chicken, mutton and kale were collected and their pH was adjusted to 7.0. The supernatant of chicken was incorporated into Cr^{3+}solution (20 mmol/L), mutton was into Al^{3+} solution (20 mmol/L) and kale was into Fe^{3+} solution (20 mmol/L) for the recovery experiments.

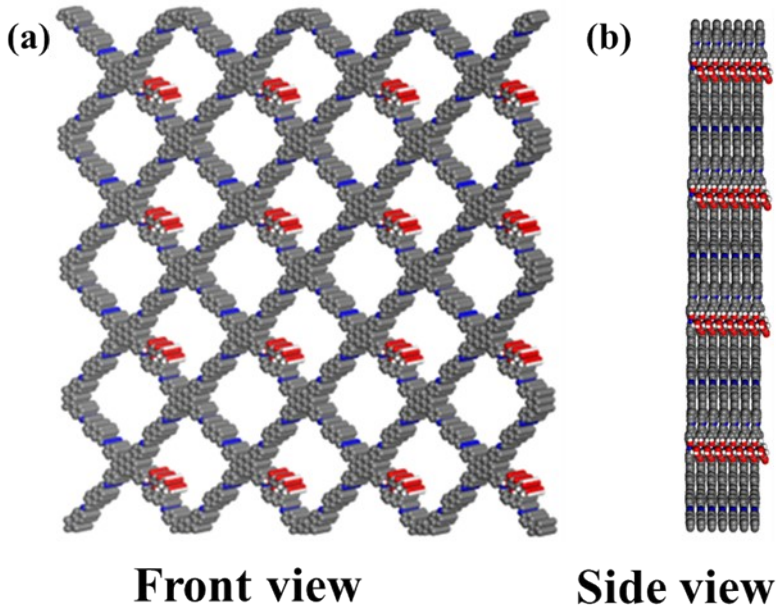

Figure S1. Eclipsed AA stacking simulated model of Ac-Py-Np COF (a) Front view, (b) Side view

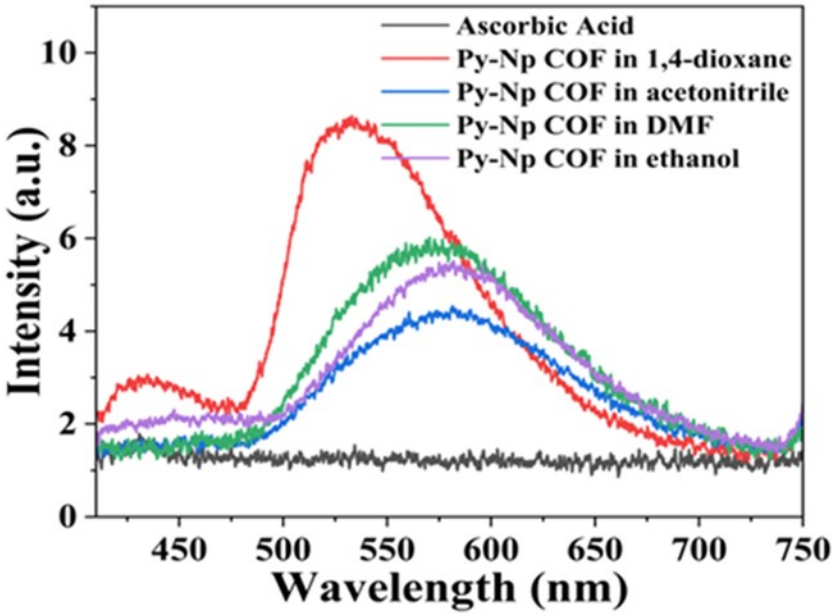

Figure S2. Fluorescence emission spectra of L-ascorbic acid in water and Py-Np COF in different solvents at excitation wavelength of 390 nm. Excitation and emission slits were kept at 5: 5

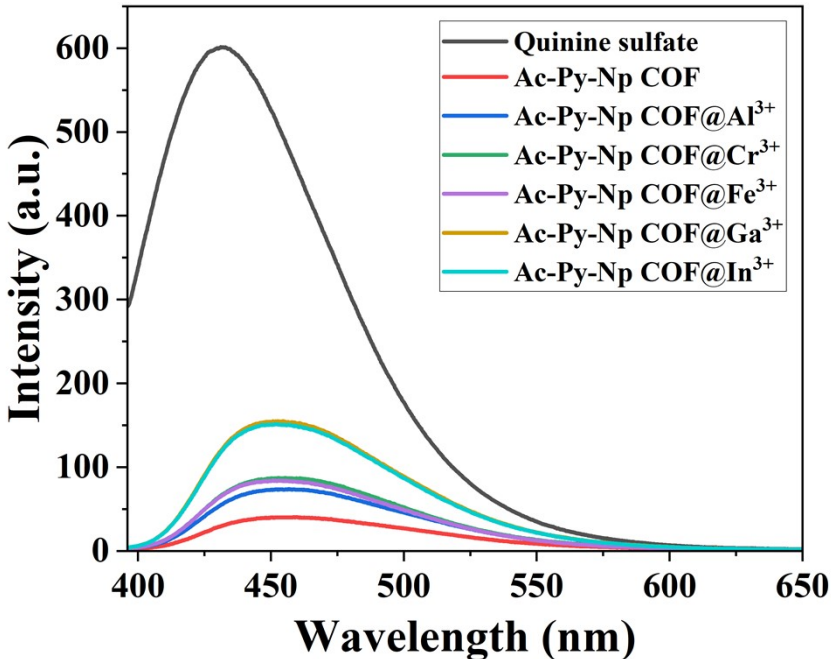

Figure S3. Fluorescence emission spectra of Quinine sulfate, Ac-Py-Np COF and its complex with trivalent metal ions at the excitation wavelength of 376 nm

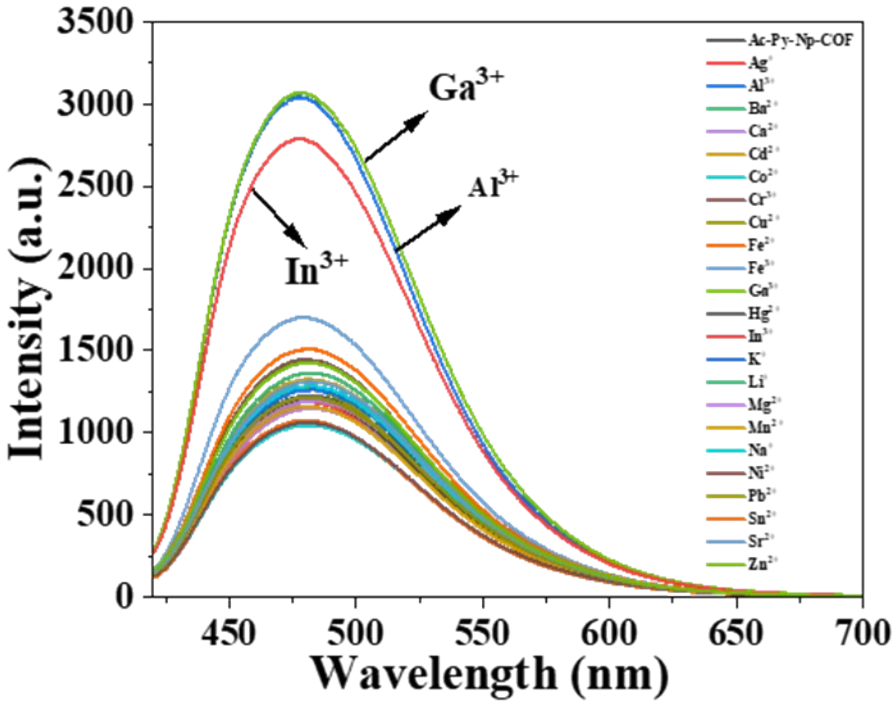

Figure S4. Fluorescence emission spectra of Ac-Py-Np COF in DMF with the addition of different metal ions at the excitation wavelength of 400 nm

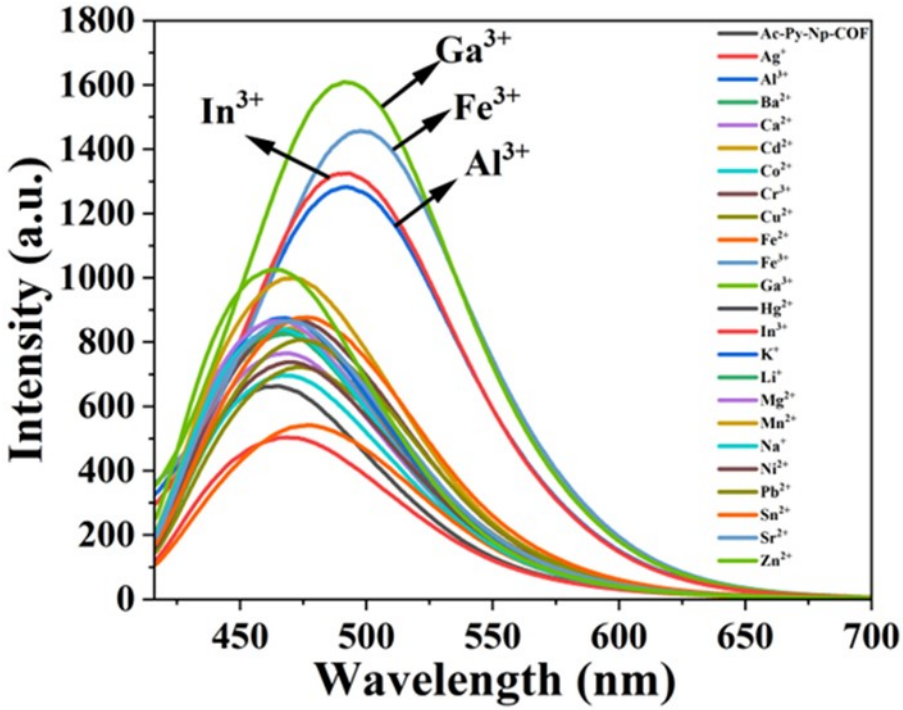

Figure S5. Fluorescence emission spectra of Ac-Py-Np COF in ethanol with the addition of different metal ions at the excitation wavelength of 396 nm

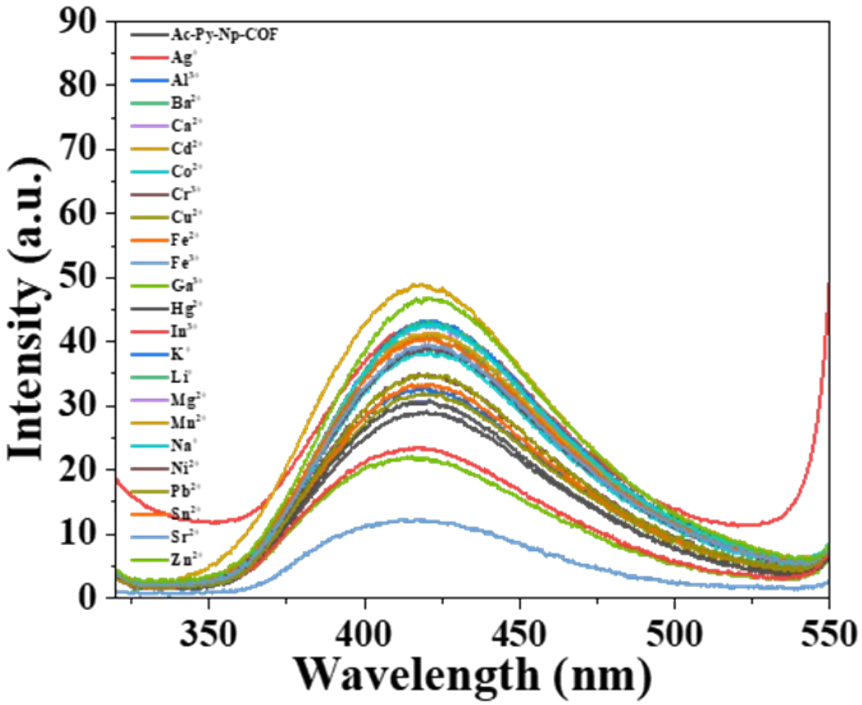

Figure S6. Fluorescence emission spectra of Ac-Py-Np COF in water with the addition of different metal ions at the excitation wavelength of 296 nm

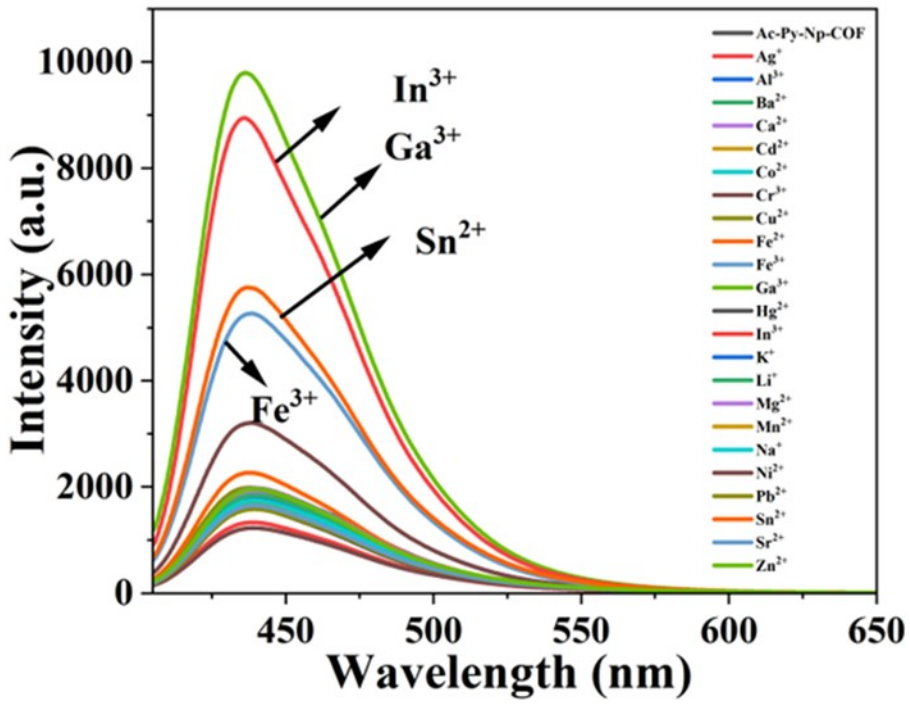

Figure S7. Fluorescence emission spectra of Ac-Py-Np COF in 1,4-dioxane with the addition of different metal ions at the excitation wavelength of 385 nm

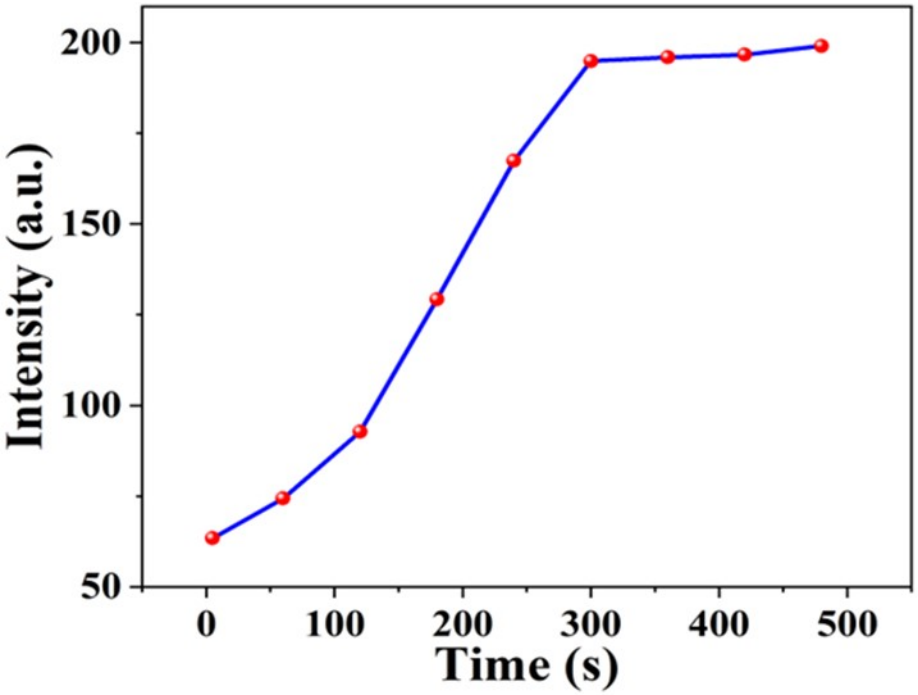

Figure S8. Response time of Ac-Py-Np COF for Al^{3+}

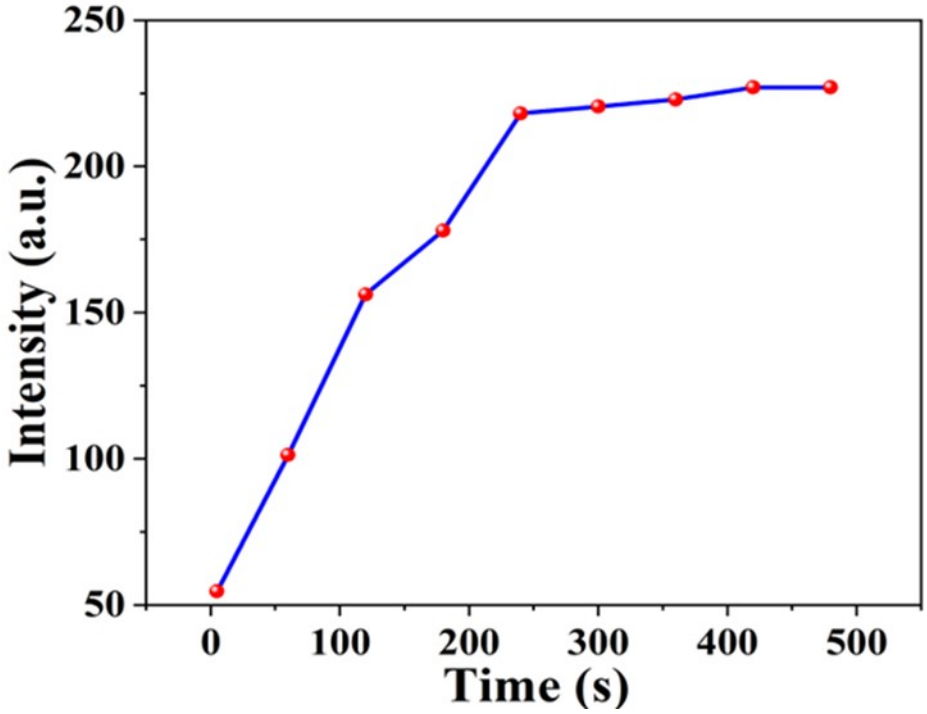

Figure S9. Response time of Ac-Py-Np COF for Ga^{3+}

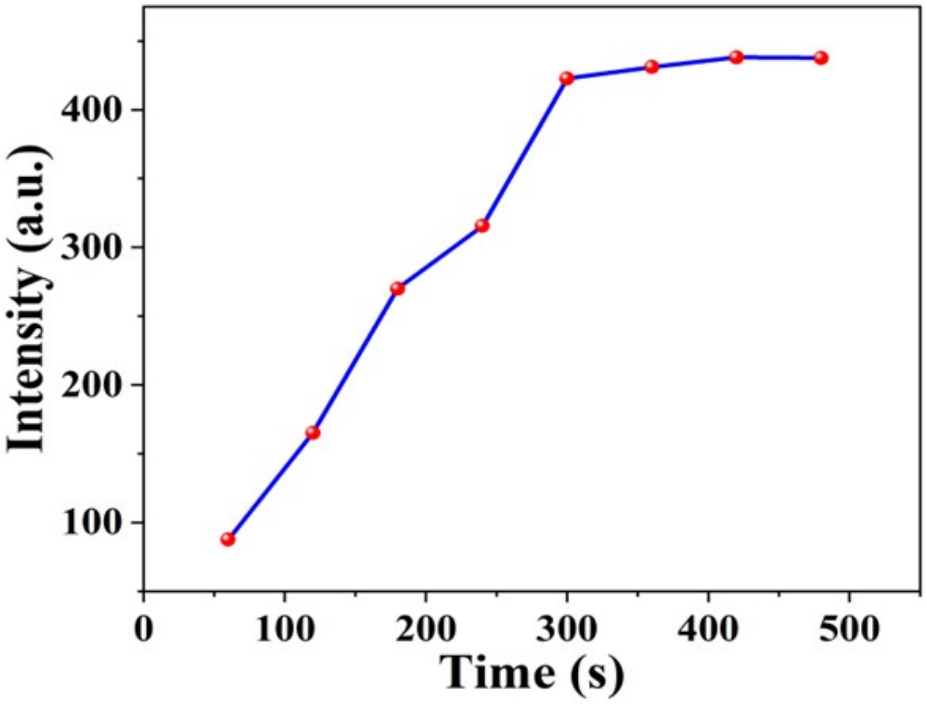

Figure S10. Response time of Ac-Py-Np COF for In^{3+}

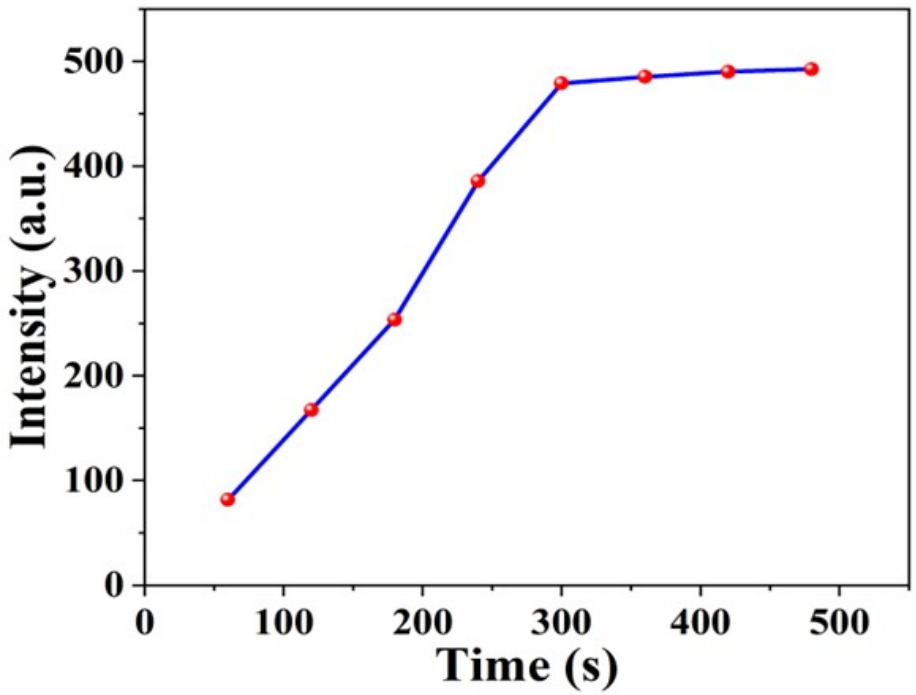

Figure S11. Response time of Ac-Py-Np COF for Cr^{3+}

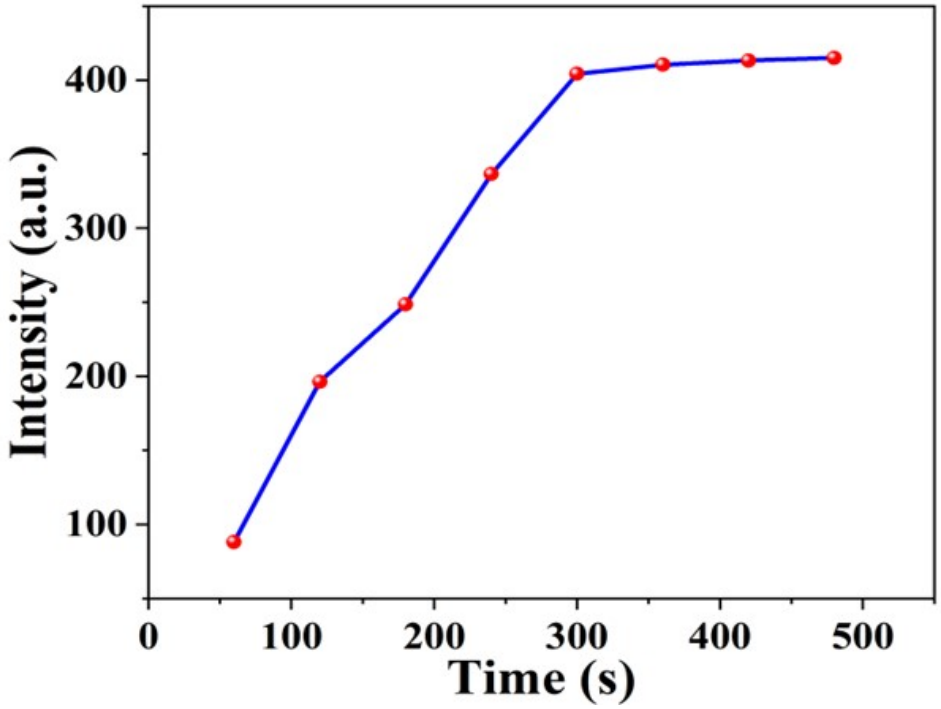

Figure S12. Response time of Ac-Py-Np COF for Fe^{3+}

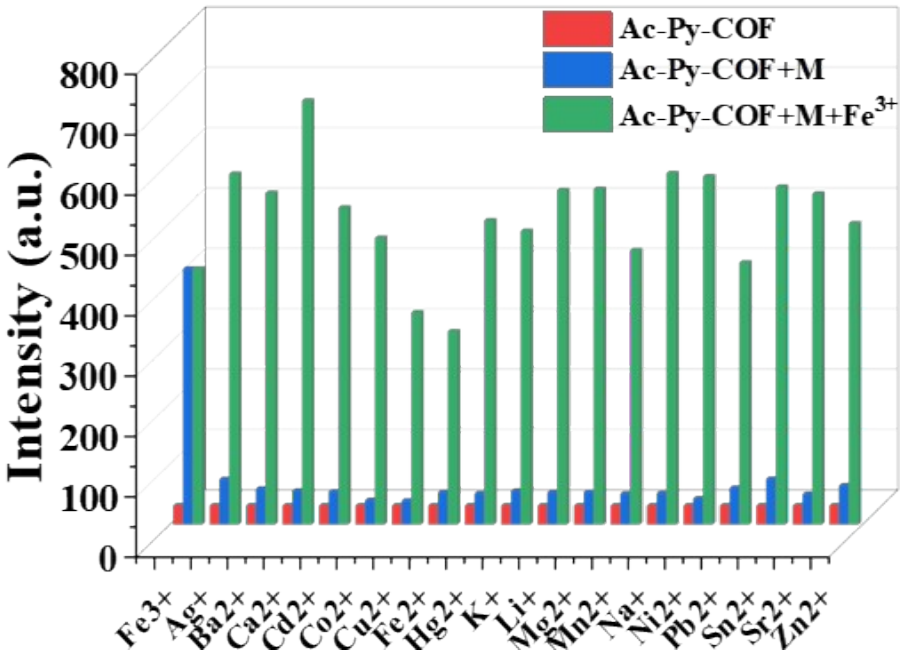

Figure S13. Anti-interference experiment of Ac-Py-COF (0.05 mg/mL) in the presence of different metal ions and Fe^{3+} ions, Excitation and emission slit was kept at 5:5

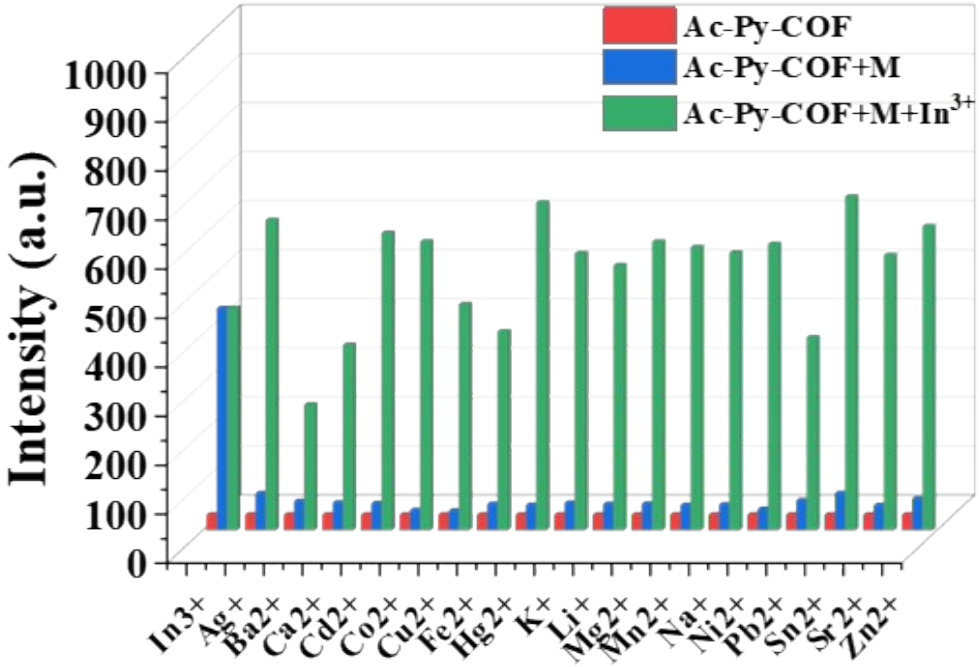

Figure S14. Anti-interference experiment of Ac-Py-COF (0.05 mg/mL) in the presence of different metal ions and In^{3+} ions, Excitation and emission slit was kept at 5:5

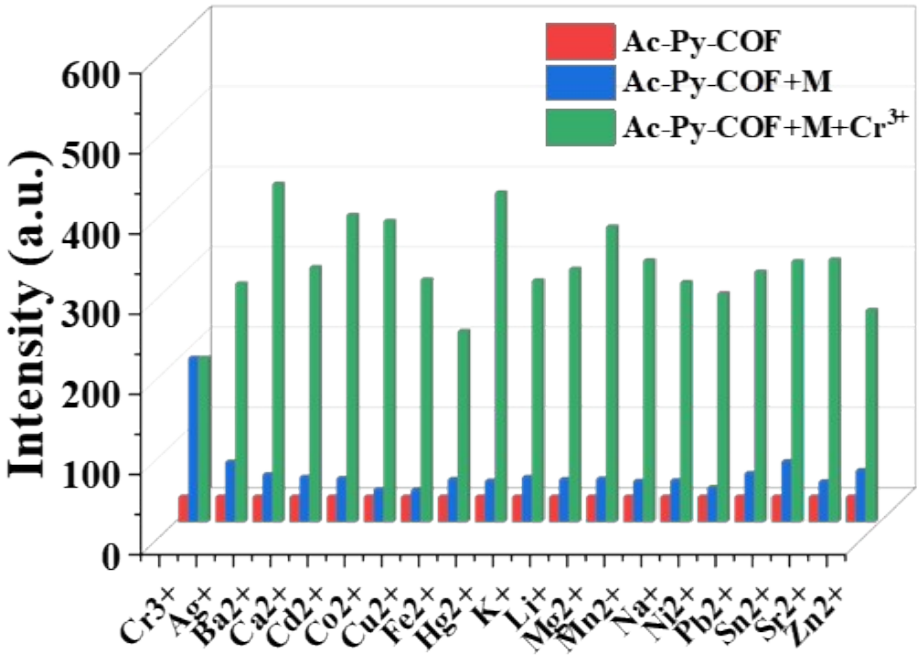

Figure S15. Anti-interference experiment of Ac-Py-COF (0.05 mg/mL) in the presence of different metal ions and Cr^{3+} ions, Excitation and emission slit was kept at 5:5

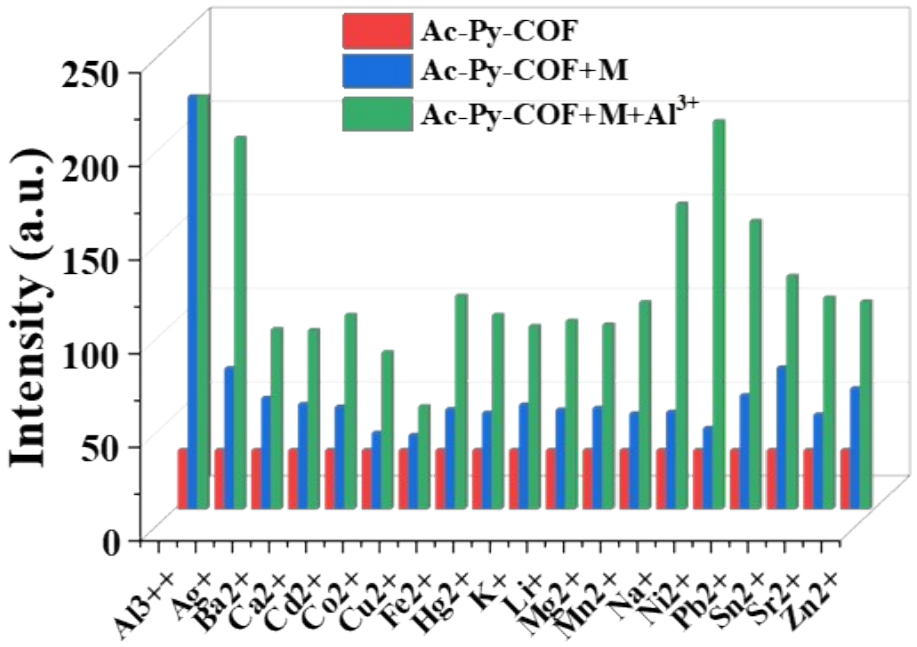

Figure S16. Anti-interference experiment of Ac-Py-COF (0.05 mg/mL) in the presence of different metal ions and Al^{3+} ions. Excitation and emission slit was kept at 5:5

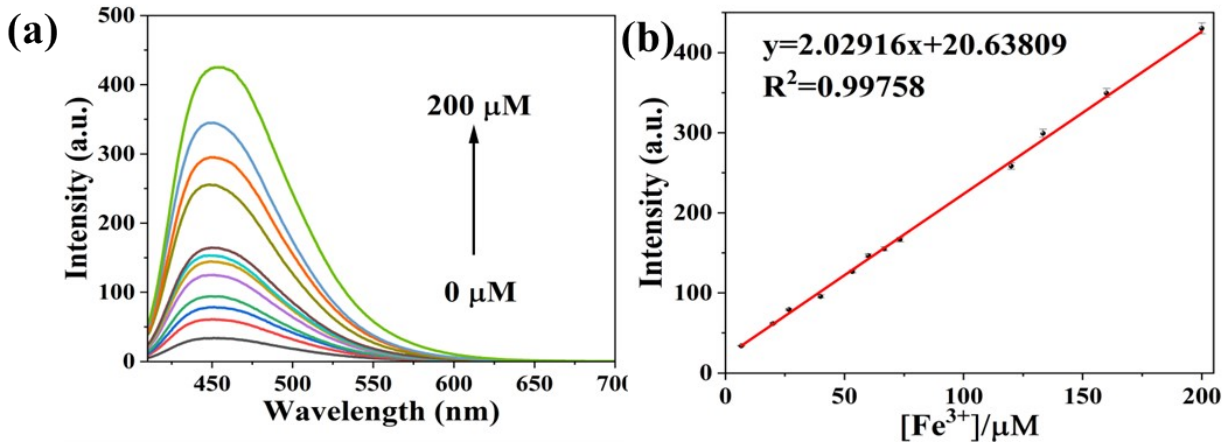

Figure S17. (a) Gradual addition of Fe^{3+} in Ac-Py-Np COF, (b) Calibration curve of Ac-Py-COF with the increasing addition of Fe^{3+} at λ_{em} = 450nm and λ_{ex} = 390 nm, Excitation and emission slit was kept at 5:5

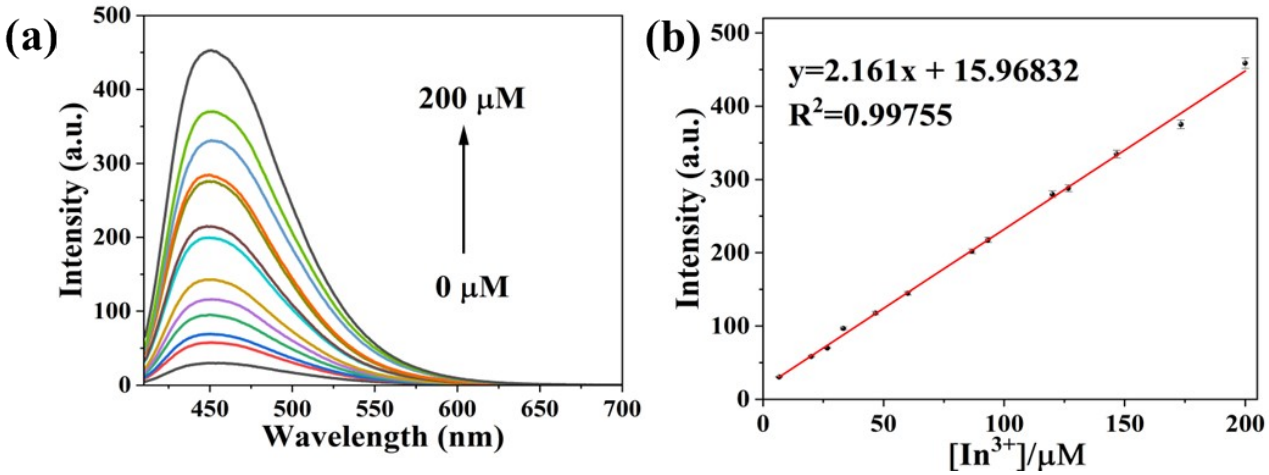

Figure S18. (a) Gradual addition of In^{3+} in Ac-Py-Np COF, (b) Calibration curve of Ac-Py-COF with the increasing addition of In^{3+} at λ_{em} = 450nm and λ_{ex} = 390 nm, Excitation and emission slit was kept at 5:5

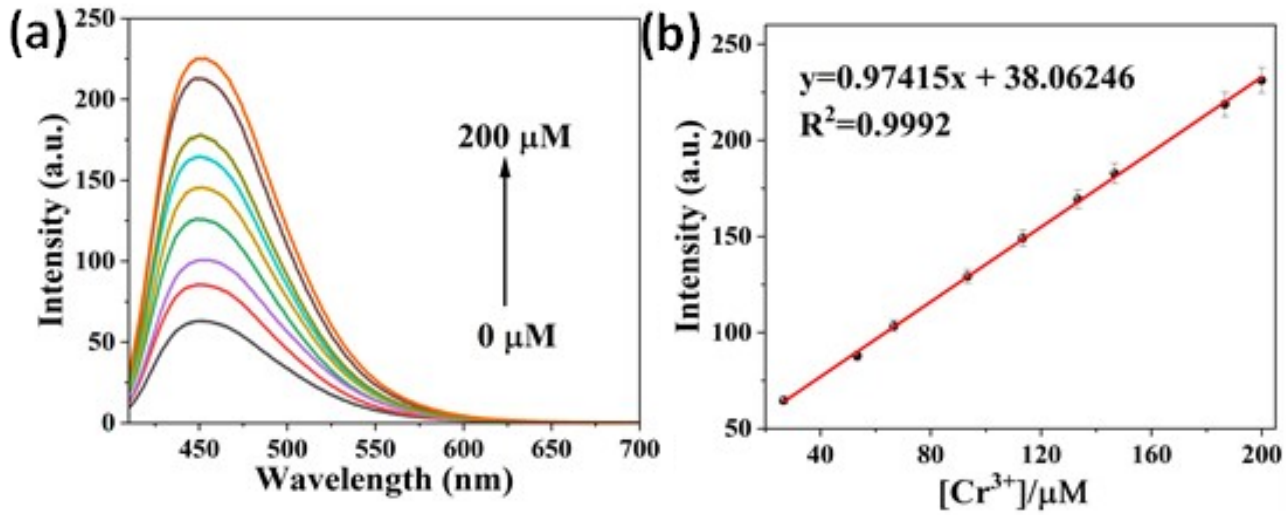

Figure S19. (a) Gradual addition of Cr^{3+} in Ac-Py-Np COF, (b) Calibration curve of Ac-Py-COF with the increasing addition of Cr^{3+} at λ_{em} = 450nm and λ_{ex} = 390 nm, Excitation and emission slit was kept at 5:5

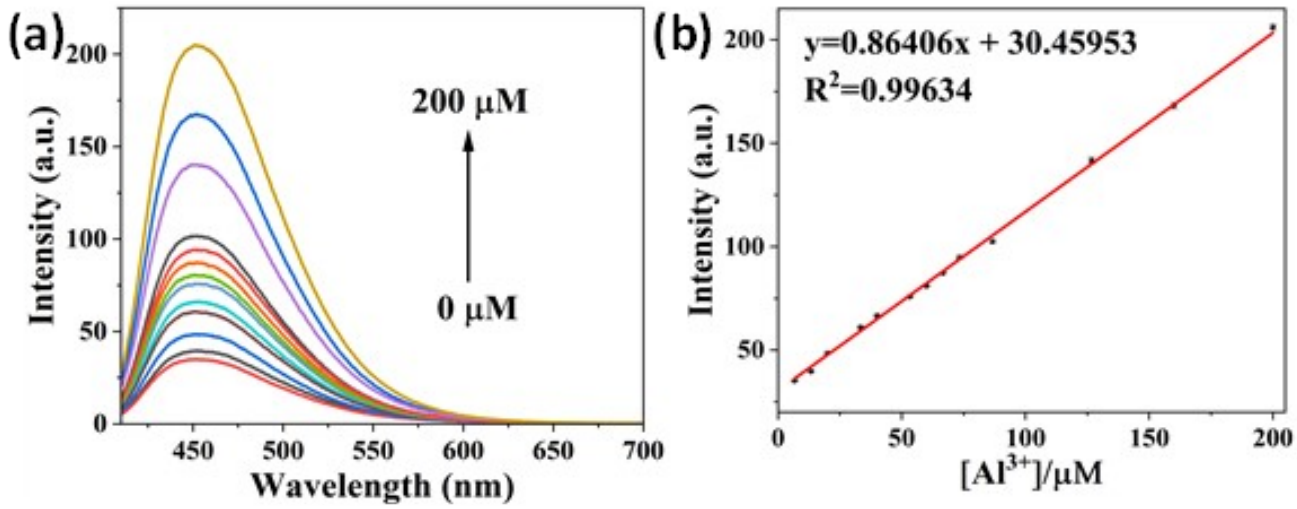

Figure S20. (a) Gradual addition of Al^{3+} in Ac-Py-Np COF, (b) Calibration curve of Ac-Py-COF with the increasing addition of Al^{3+} at λ_{em} = 450nm and λ_{ex} = 390 nm, Excitation and emission slit was kept at 5:5

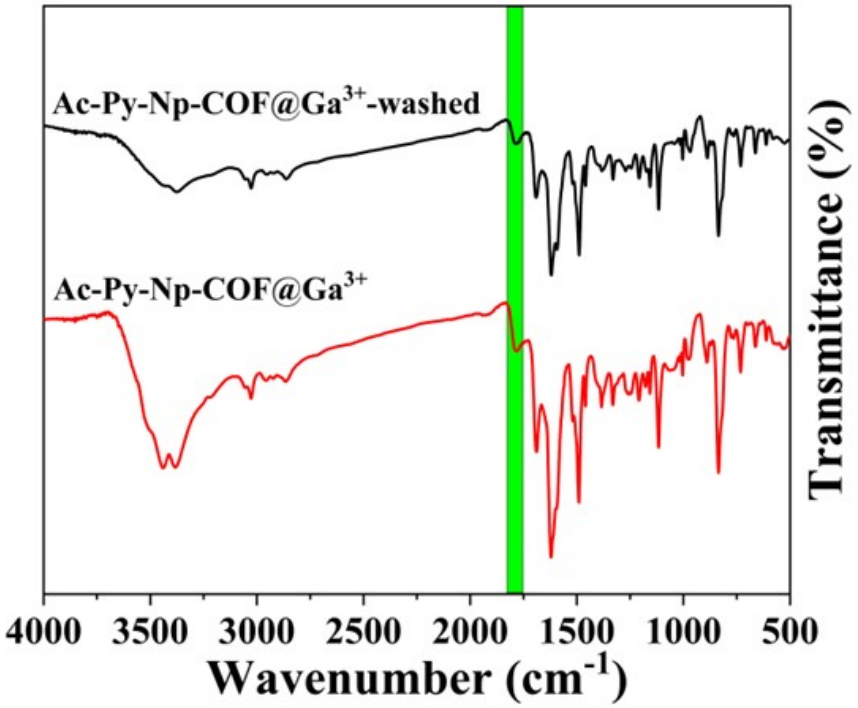

Figure S21. FT-IR of Ac-Py-Np COF@Ga^{3+} and Ac-Py-Np-COF@Ga^{3+}

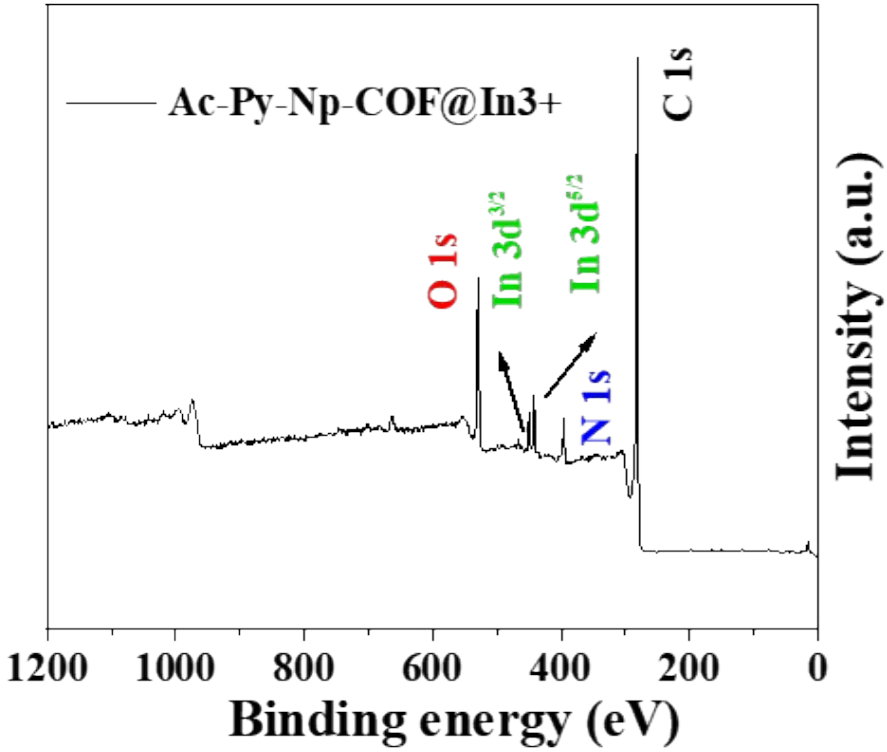

Figure S22. Full XPS of Ac-Py-Np-COF@In^{3+}

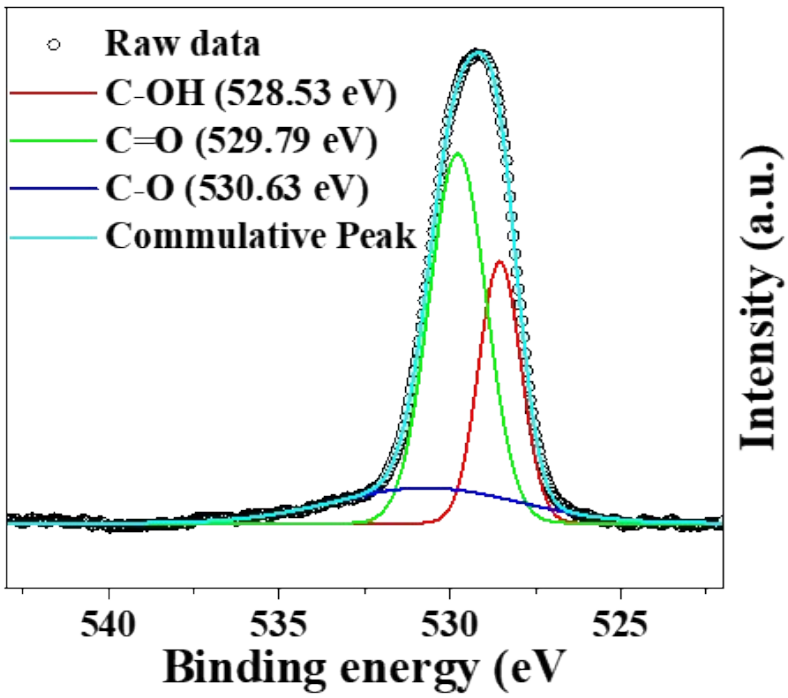

Figure S23. XPS of O 1s of Ac-Py-Np COF

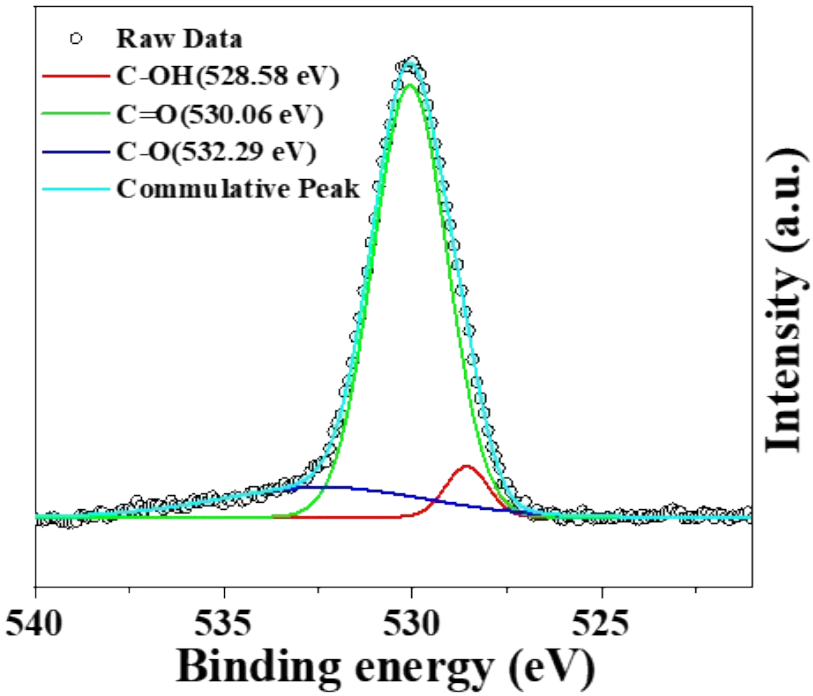

Figure S24. XPS of O 1s of Ac-Py-Np-COF@Ga^{3+}

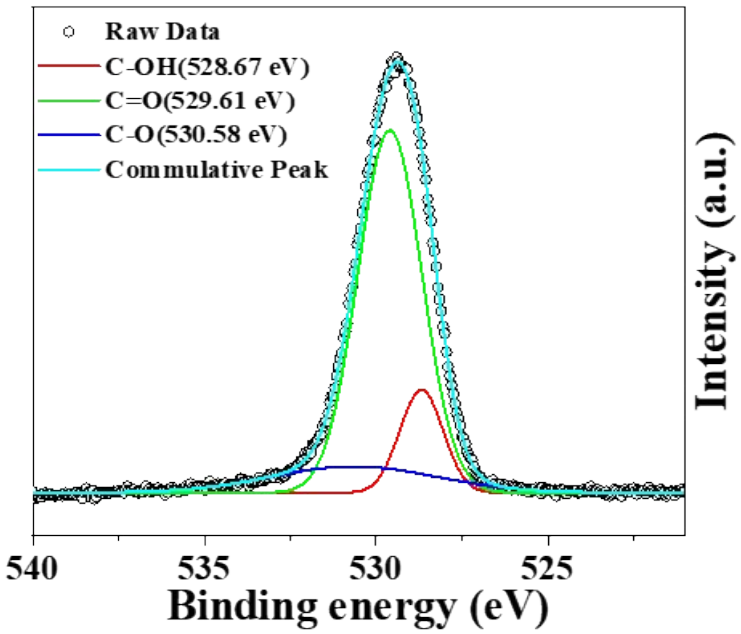

Figure S25. XPS of O 1s of Ac-Py-Np-COF@In^{3+}

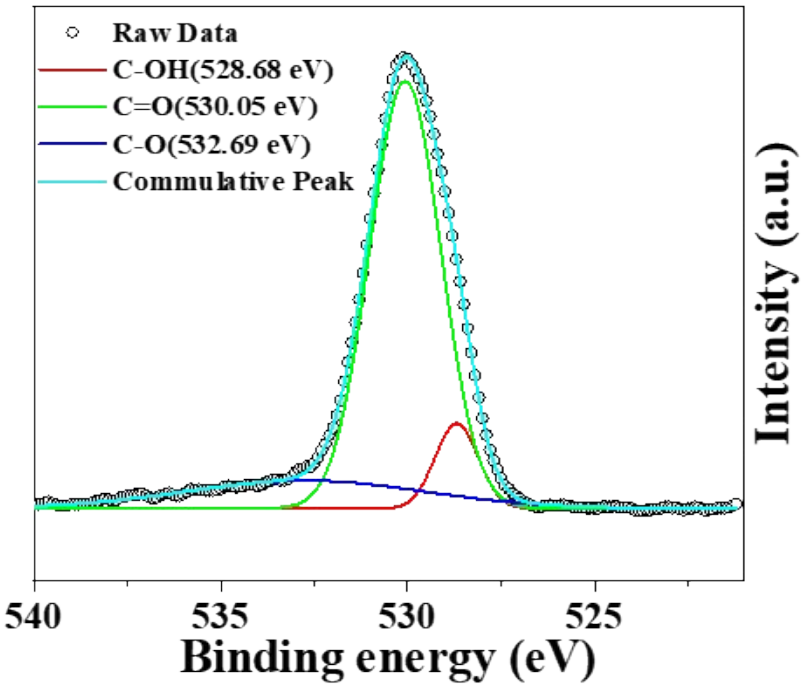

Figure S26. XPS of O 1s of Ac-Py-Np-COF@Ga^{3+}

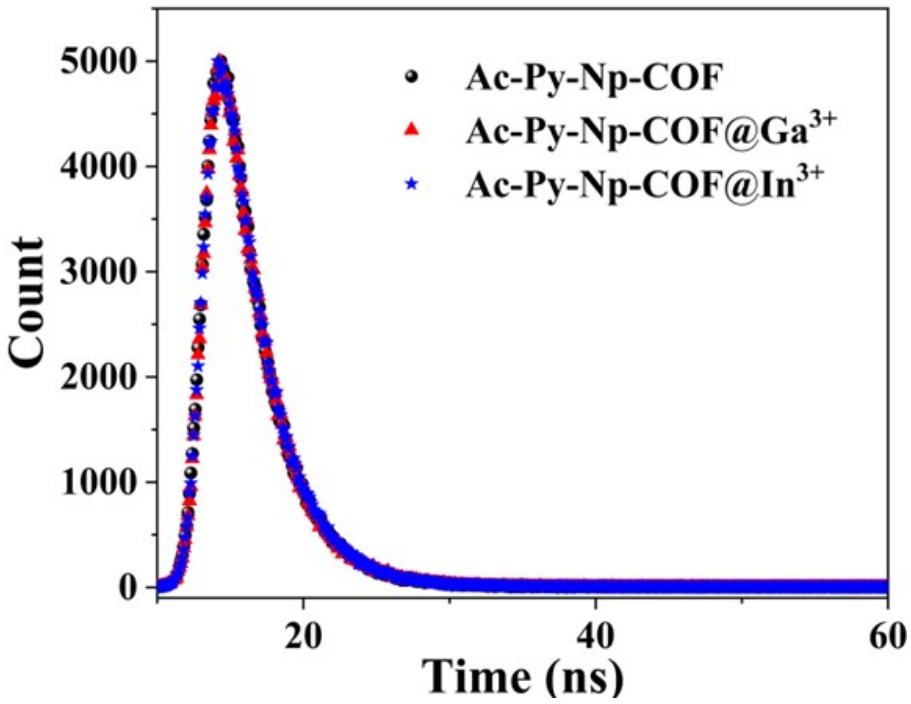

Figure S27. Fluorescent lifetime experiment of Ac-Py-Np-COF, Ac-Py-Np-COF@Ga^{3+} and Ac-Py-Np-COF@In^{3+}

Table 1. Comparison of different aspects of Ac-Py-Np COF with other chemosensors to detect trivalent metal ions

Chemosensors	Metal ions	Linear range (μM)	LOD	Application	Response time (s)	References
LB3	Ga^{3+}	0-150	4.42×10^{-9} M	Tap water		
	In^{3+}	0-80	1.99×10^{-11} M		-	[1]
LB3[In3+]	Fe^{3+}	0-80	1.67×10^{-8} M			
LN	Al^{3+}	0-140	1.39×10^{-8}	Test strip and	30 s	
[LN + Al3+]	Fe^{3+}	0-75	1.26×10^{-8}	bio-imaging	30 s	[2]
Sensor 1	In^{3+}	0-12	5.89×10^{-6} M	Test strip	-	
	Al^{3+}		0.30×10^{-6} M			[3]
	Al^{3+}	0-42	6.97×10^{-9} M	Living cell		
HL-CHO	Cr^{3+}	0-42	15.80×10^{-9} M	imaging	-	[4]
	Fe^{3+}	0-42	14.00×10^{-9} M			
	Al^{3+}	0-10	13×10^{-7} M	Water samples		
DHSF	Fe^{3+}	0-20	0.32×10^{-7} M			[5]
	Cr^{3+}	0-6	7.2×10^{-8} M		-	
	Al^{3+}	0-200	1.57×10^{-6} M	Mutton	300 s	
	Ga^{3+}	0-200	0.58×10^{-6} M	Tap Water	240 s	
Ac-Py-Np	In^{3+}	0-200	0.63×10^{-6} M	Tap Water	300 s	This work
COF	Cr^{3+}	35-200	1.40×10^{-6} M	Chicken	300 s	
	Fe^{3+}	0-200	0.67×10^{-6} M	Kale	300 s	

References

[1] Y. Zhang, B. Li, A multifunctional selective fluorescent chemosensor for detection of Ga^{3+}, In^{3+} and Fe^{3+} in different solvents, Journal of Molecular Structure, 1250(2022).
[2] B. Zhao, A.-P. Luo, L.-P. Liu, X. Bai, Y. Sun, Z.-P. Deng, et al., A non-fluorescent group-based “off-on-off” chemosensor for detection of Al^{3+} and Fe^{3+} and zebrafish bioimaging, Journal of Molecular Structure, 1327(2025).
[3] S.Y. Lee, M. Yang, C. Kim, A dual target chemosensor for the fluorometric detection of $In^{(3+)}$ and colorimetric detection of $Fe^{(3)}$, Spectrochim Acta A Mol Biomol Spectrosc, 205(2018) 622-9.
[4] A. Roy, S. Das, S. Sacher, S.K. Mandal, P. Roy, A rhodamine based biocompatible chemosensor for $Al^{(3+)}$, $Cr^{(3+)}$ and $Fe^{(3+)}$ ions: extraordinary fluorescence enhancement and a precursor for future chemosensors, Dalton Trans, 48(2019) 17594-604.
[5] J. Wang, Y. Gao, Y. Zhang, D. Xu, Z. Li, Y. Su, et al., Multisite-complexation-regulating solvent-dependent monomolecular chemosensor for the quantification of Fe^{3+}/ClO^{-} and rapid detection of $Al^{3+}/Cr^{3+}/Cu^{2+}$, New Journal of Chemistry, 49(2025) 9133-44.